H. M. El-Batsh et al., Three Dimensional Heat Transfer Characteristics through a Linear Gas Turbine Cascade, pp. 947 - 970

THREE DIMENSIONAL HEAT TRANSFER CHARACTERISTICS THROUGH A LINEAR GAS TURBINE CASCADE

H. M. El-Batsh *, S. A. Nada, S. N. Abdo, A. Mohamed

Mechanical Engineering Department, Benha Faculty of Engineering, Benha University, Egypt

Received 1 September 2012, accepted 13 November 2012

ABSTRACT

This study presents experimental and numerical investigation for three-dimensional heat transfer characteristics in a turbine blade. An experimental set-up was installed with a turbine cascade of five blade channels. Blade heat transfer measurements were performed for the middle channel under uniform heat flux boundary conditions. Heat was supplied to the blades using twenty-nine electric heating strips cemented vertically on the outer surface of the blades. Distributions of heat transfer coefficient were obtained at three levels through blade height by measuring surface temperature distribution using thermocouples. To understand heat transfer characteristics, surface static pressure distributions on blade surface were also measured. Numerical investigation was performed as well to extend the investigation to locations other than those measured experimentally. Three-dimensional non-isothermal, turbulent flow was obtained by solving Reynolds averaged Navier Stokes Equations and energy equation. The Shear stress Transport k-ω model was employed to represent turbulent flow. It was found through this study that secondary flow generated by flow deflection increases heat transfer coefficient on the blade suction surface. Separation lines with high heat transfer coefficients were predicted numerically with good agreement to the experimental measurements.

Keywords: Gas turbine blades, Heat transfer, Secondary flow, Computational fluid dynamics

1. Introduction

The performance of gas turbine engines is determined by its specific work and thermal efficiency which are improved by increasing combustor gas exit temperature. However, increasing combustor exit temperature increases the thermal load on the first stage of a gas turbine engine. Consequently, heat transfer characteristics are required for engines safe operation. In addition, effective cooling of turbine blades is required to reduce thermal load and allow safe and effective operation at high levels of gas temperatures. To optimize blade cooling, exact understanding of surface heat transfer of a turbine blade is necessary. Heat transfer mechanism in gas turbine blades is very complicated due to the complexity of flow pattern around the blades. Flow in turbine cascades is characterized by different flow features which include accelerating flow on blade pressure side and accelerating, decelerating flow on blade surface. In addition, the passage flow is characterized by boundary layer effects, secondary flow generated by the passage pressure gradients, and vortical flow structures such as the leading edge horseshoe vortices, affects the three-dimensional heat transfer in gas turbine blades.

Laboratory measurements are available in the literature and conducted to understand two-dimensional heat transfer at blade mid-span. Extensive investigation on mid-span heat transfer of a turbine blade has been performed by Arts et al.[1]. They studied fluid flow and

* Corresponding Author.
E-mail address: helbatsh@yahoo.com

heat transfer in a highly loaded transonic linear turbine guide vane cascade at the design incidence. A set of experimental studies were performed to investigate the effect of Reynolds number and Mach number as well as free stream turbulence intensity on heat transfer characteristics of a turbine cascade. Later, numerous numerical studies had used the measured data obtained by Arts et al. [1] to evaluate the accuracy of their two-dimensional numerical calculations [2-10].

Researchers used also data obtained by Arts et al. [1] for prober selection of turbulence models and to investigate the effect of turbulence intensity, length scale on heat transfer on turbine blades (e.g. Garg and Ameri[11]).

Two-dimensional measurements are very useful for understanding blade heat transfer at mid-span and provide useful data for numerical model validation. However, two dimensional study cannot simulate the real heat transfer mechanism in a gas turbine blade where three-dimensional flow is developed in turbine blade passages due leading edge horseshoe vortices. Langston et al. [12], Sieverding [13] and Wang et al. [14] provided complete overview on the basic aspects of secondary flow in turbine blade passage. Secondary flow affects the aerodynamic performance of a turbine cascade and changes heat transfer characteristics from the hot fluid to the blade and end-wall surfaces.

Figure 1 shows the features of the secondary flow generated in turbine cascades as presented by Wang et al. [14]**.** Due to the blockage presented by the leading edge, the incoming end-wall boundary layer is subjected to a stagnation pressure gradient. This causes the boundary layer to undergo three-dimensional separation and to roll up into a horseshoe vortex, as illustrated. The legs of the horseshoe vortex pass to either side of the blade. The suction-side leg travels around the blade and its lift-off line later intersects the blade suction surface. The pressure side leg moves into the blade passage and merges with the main passage vortex, which itself moves across to the suction surface of the neighboring blade under the influence of the passage pressure field. The figure indicates also that corner vortices are generated near the end-wall.

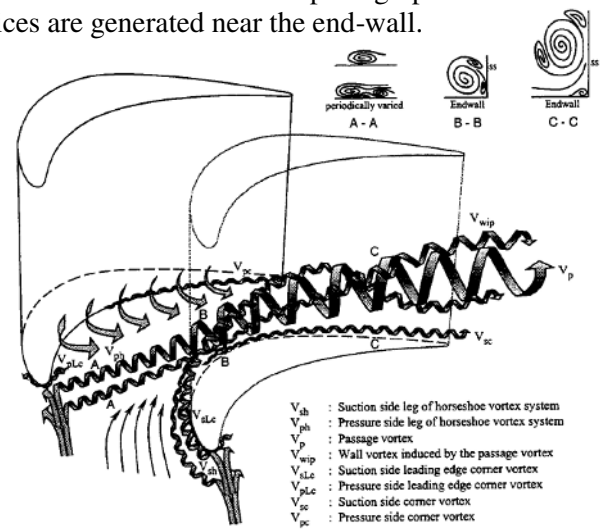

Fig. 1. Secondary flow model by Wang et al. [14]

Giel et al. [15] studied the effect of Reynolds number, exit Mach number, and inlet turbulence intensity on three-dimensional heat transfer using experimental measurements. The results were compared to numerical calculations using three-dimensional Navier-Stokes code. The comparison illustrated regions of good agreement while other regions need modeling improvement. The results also showed that heat transfer near end-wall suction surface region increased by secondary flow. Pecnik et al. [16] presented three dimensional numerical investigations on a transonic turbine guide vane using different turbulence models on the predication of heat transfer and secondary flow effects. Garg and Ameri [11] performed numerical simulation using k-ωmodel and a shear stress transport (SST) k-ωmodel and compared their results with heat transfer measurements on a transonic turbine blade of Giel et al.[15]. The results showed that the k-ω model and SST model compare well on pressure side of the blade and leading edge. For the suction side the SST model resolve the passage vortex better yielding a better comparison with experimental

data than $k-\omega$model. Johan et al. [17] predicted numerically the secondary flow downstream of a highly loaded low pressure turbine outlet guide vane cascade. Papa [18] studied the effect of secondary flow on heat transfer on blade and hub wall surfaces of a gas turbine engine. The measurements are performed in a linear cascade composed of five blades. Tests are conducted at a Reynolds number of 6×10^5. The (RANS) carried out to simulate the flow and heat/mass transfer using SST k-ω model is evaluated through a comparison with the experimental data. Results show that the SST k-ωmodel predicted well heat transfer on the airfoil surface and formations and development of the horseshoe vortex. The heat transfer on the end wall was also well predicated.

Lee and park [19] Investigate the effect of incidence angle on the end-wall heat transfer, Surface flow visualization and heat transfer measurements are carried out at the inlet

Reynolds number of 2.78×10^5, and for incidence angles of -10^o, -5^o, 0^o, 5^o, and 10^o. The results show that in the negative incidence case, the mass transfer is less influence by the leading edge horseshoe vortex and by suction side corner vortex. Lynch et al. [20] studied the effect of three dimensional end-wall non-axisymmetric contouring on the end-wall heat transfer for a low pressure turbine blade. End-wall oil flow visualization indicated that the passage vortex strength is reduced for contoured end wall geometry as compared with flat end-wall. Lynch et al. [21] used the commercial computational fluid dynamic software FLUENT to simulation the effect of flat end-wall and three dimensional non-axisymmetric contoured end-wall on the end-wall heat transfer for a low pressure turbine blade. They found that the heat transfer for a non-axisymmetric contour relative to a flat end-wall showed fair agreement to the experiment.

Morata et al. [22] provided 3D numerical investigation to predicated the wall heat transfer distribution in a highly loaded turbine guide vane with RANS and two LES approaches (structured and unstructured). The predicated heat transfer from both RANS and LES were compared by the experimental measurements Arts et al.[1].

The literature review show that the previous studies had focused on investigation of performance of different numerical techniques and turbulence models rather than providing complete overview on the effect of the secondary flow through turbine cascades. The aim of the present study is to investigate the three-dimensional heat transfer and flow characteristics through a turbine cascade. The study aims also to understand the process of heat transfer and to investigate the parameters affecting heat transfer in turbine blades. Effect of secondary flow on the distribution of the convection heat transfer coefficient is also examined. Flow and heat transfer characteristics are examined at different Reynolds numbers.

2. Experimental technique

2.1. Experimental set-up

The experimental set-up used in the present study was constructed in the fluid mechanics laboratory, Benha Faculty of Engineering, Benha University, Egypt. It basically consists of a low-speed wind tunnel equipped with a nozzle and a test section. The wind tunnel is 4.5 m long and has a cross-section of 0.6m × 0.6. It is equipped with a centrifugal fan driven by a 10 HP three-phase AC electric motor. Air velocity through the wind tunnel is controlled by a throttling mechanism at fan inlet. A contraction nozzle was used to reduce the cross-section to fit the test section dimensions and to provide uniform flow at inlet to test section.

The test section was made of Plexiglas with inlet dimension of 0.6m×0.173m and outlet dimension of0.331m×0.173m as shown in figure 2. The blade profile is similar to that used by Langston et al. [12] with blade chord length of 0.168 m and cascade parameters as given in table 1. Figure 3 shows the turbine cascade with summary of geometrical parameter is given in table 1.To obtain periodic flow which is essentially in linear cascade measurements, the linear cascade used in the present study contains six blades to create five flow passages as shown in Figure 1. This is similar to the linear cascade of Arts et al. [1] where periodic flow was obtained using five blades. The blades were fabricated from beech wood by using CNC machine. The blade coordinates were supplied to the machine and the blade profile was obtained with accuracy of 1μm. Flow and heat transfer measurements were obtained for the middle blade channel to avoid end effects. The two center blades were instrumented for measurements and can be replaced. Two-sets of instrumented blades were prepared for individual surface static pressure and heat transfer measurements. The first set allowed surface static pressure measurements while the second set allowed heat transfer measurements.

2.2. Blade static pressure measurements

The two blades forming the central flow channel were instrumented with static pressure tapping for surface pressure measurements. Pressure taps were made of stainless steel needles with inner diameter of 1.3mm and outer diameter of 1.6mm connected to a digital

micro-manometer via plastic tubes of 1.3 mm inside diameter, 2 mm outside diameter, and 1.5 m long. The pressure taps were placed at levels of 0.5, 0.25, and 0.875 blade span as shown in figure 4a. There were 19 pressure taps located at each level through blade height; 9 taps on the blade pressure surface and 10pressure taps on the blade suction surface. The taps were connected to the digital micro-manometer with full scale of 3700 Pa and accuracy of 0.3% of the full scale.

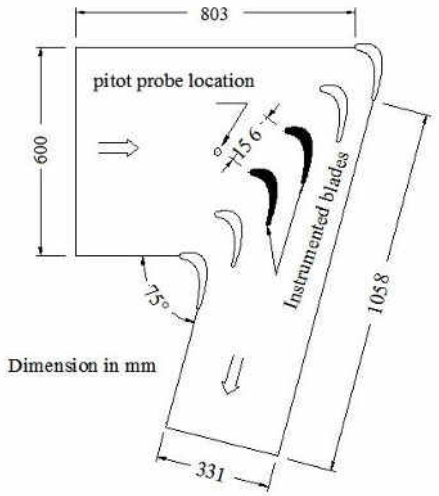

Fig. 2. Schematic diagram of test section

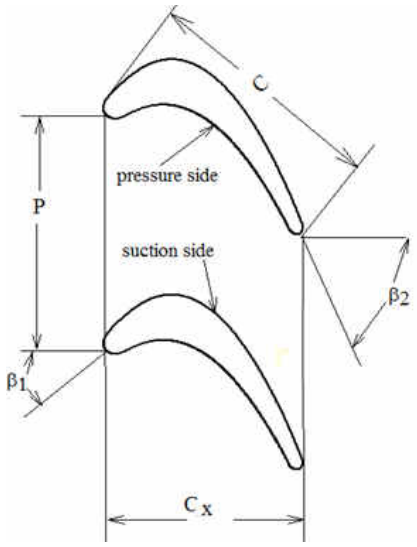

Fig. 3. Diagram illustrating cascade parameters

Table 1.
Cascade parameters

Number of blades	6
Blade chord length, C [mm]	168
Blade axial chord, C_x [mm]	144
Blade pitch, P [mm]	156
Blade height, H [mm]	173
Blade inlet angle, β_1[°]	40
Blade exit angle, β_2[°]	65
Incidence angle, i [°]	0
Stagger angle, γ [°]	35

2.3. Heat transfer instrumented blade

Heat transfer measurements were conducted under uniform heat flux was supplied to the blades using 29 nickel chrome boundary conditions on the blade surface. Heat electric heating resistance strips cemented vertically on the outer surface of the blades with 2mm spacing between adjacent strips. The strips were connected together in series using copper bus bars. The strips dimensions were 173 mm long, 10 mm wide and 0.15 mm thick. The heat transfer instrumented blade for suction side shown in figure 4b.The electric power was supplied to the resistance strips through a DC power supply. The required heat flux was maintained by controlling the current and voltage supplied to the strips. Sixty calibrated thermocouples of Chromel-alumel were soldered on the foil strips at three different levels along blade height (0.5,0.25, and 0.875 H). The thermocouples were connected to a digital temperature recorder with 0.1°C resolution through a set of selector switches.

(a) Blade with static pressure tapping

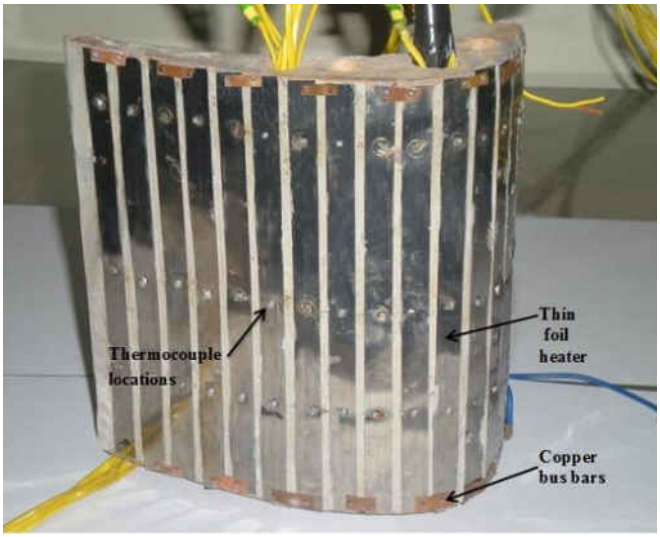

(b) Heat transfer instrumented blade

Fig. 4. Instrumented blades

2.4. Measurement procedure

A calibrated five-hole pressure probe with a tip diameter of 3 mm was used to measure the flow field at the inlet to the cascade. The pressures at the five holes were measured in order to determine flow conditions at the probe tip using indirect method. The relationship between the measured pressures and stagnation pressure, velocity and flow angles was obtained from the calibration charts. Complete information on the measurements using five-hole probe and calibration procedure of the used probe can be found in El-Batsh [23].The experiments were conducted at inlet velocities of 10, 15, and 20 m/s corresponding to blade inlet Reynolds numbers (Re) of 106000, 159000, and 212000, respectively. The blade inlet Reynolds number is given by:

$$Re = \frac{\rho U_1 C}{\mu}$$

where U_1 is the inlet flow velocity, $C$is the blade chord length, ρ is the air density and μ is the fluid viscosity.

The inlet turbulence intensity was calculated using 2000 instantaneous velocity measurements.

2.5. Data analysis

Surface static pressure measurements were expressed as static pressure coefficient defined based on the inlet velocity as:

$$C_p = \frac{P_s - P_1}{0.5\rho {U_1}^2} \quad (1)$$

where P_s is local static pressure distribution on the blade surface, P_1 is the inlet static pressure and U_1 is the inlet velocity.

The local heat transfer coefficient was calculated as:

$$h = \frac{q''}{T_w - T_\infty} = \frac{q''_{gen} - q''_{loss}}{T_w - T_\infty} \quad (2)$$

where q'' is the net local convective heat flux from the foil strips, q''_{gen} is the generated heat flux from voltage-current measurements, $q''_{loss}$is heat flux loss by radiation and by conduction. T_w is the local steady state strip surface temperature, and $T_\infty$is the uniform temperature at inlet of the cascade. The local Nusselt number Nu was calculated from

$$Nu = \frac{hC}{K} \quad (3)$$

Where h is the local heat transfer coefficient, C the blade chord length, and K is air thermal conductivity.

The loss heat flux by conduction was obtained by measuring heat loss from the test blade at the condition without air flow through blade channel. This was done by supplying several different input powers and getting a correlation between conduction heat loss and individual foil temperature (T_w) at steady state. The local radiation loss was estimated using a foil emissivity of 0.95.

$$q"_{loss} = \epsilon\sigma(T^4{}_W - T^4{}_\infty) + q"_c \quad (4)$$

The total heat loss was about15 percent of the heat generated in the foil. The conduction and radiation heat loss were 6% and 9%, respectively.

2.6. Measurements uncertainty

The calculation of the Nusselt number can be represented by the following form

$$Nu = f(x_1, x_2, \ldots . x_n) \quad (5)$$

Where x_1 to x_n are all the variables that affect the experimental determination of Nu.

The uncertainty ΔNuin the value of $Nu$was estimated based on the procedure of Holman and Gajda [24] and is expressed as follows

$$\Delta Nu = \sqrt{\sum_{i=1}^{n}\left(\frac{\partial Nu}{\partial x_i}\Delta x_i\right)^2} \quad (6)$$

Where Δx_i is the uncertainty in the variablex_i. The uncertainty in the various variables used in the determination of the Nusselt number were: 0.25 % for the electric current, 0.25% for the electric volt,0.2ºC for temperature measurements, 0.0001 m for the distance, 0.5% for the air thermal conductivity, and 5% for the emittance of the heater strips. It was found that the uncertainty of Nu ranges from 4.8 % to 8.6%.

3. Numerical procedure

Numerical studies have been carried out using commercial CFD codes, namely FLUENT 6.3.26to understand different flow features and to obtained complete information on heat transfer coefficients on the blade surface. Heat transfer and fluid flow characteristics were obtained by solving the flow governing equations namely continuity, momentum, energy and turbulence. The flow is considered steady and incompressible since the flow Mach number is rather small. The computational domain is defined by the inlet plane which was placed at a distance of 0.7 axial chord upstream of the blade leading edge. The outlet plane was selected at a distance of one axial chord downstream of the blade trailing edge figure 6.

The calculations were performed for blade half-span considering the mid-span is a symmetry plane. Periodic boundaries were considered to account for the periodic flow through the cascade.

3.1. Governing equations

The governing equations for incompressible flow are given by

$$\frac{\partial \bar{u}_i}{\partial x_i} = 0, \tag{7}$$

$$\rho \frac{\partial \bar{u}_i \bar{u}_j}{\partial x_i} = -\frac{\partial \bar{p}}{\partial x_j} + \frac{\partial}{\partial x_i}\left[\mu\left(\frac{\partial \bar{u}_i}{\partial x_j} + \frac{\partial \bar{u}_j}{\partial x_i}\right) - \overline{\rho \grave{u}_i \grave{u}_j}\right], \tag{8}$$

$$-\frac{\partial(\rho E)}{\partial t} + \frac{\partial(\rho u_j E)}{\partial x_j} = \frac{\partial}{\partial x_j}\left(\frac{\mu}{Pr}\frac{\partial E}{\partial x_j}\right) + \frac{\partial}{\partial x_j}(u_j \tau_{ij}) \tag{9}$$

where the velocities $\bar{u}_i$ are mean values, $\grave{u}_i$ are the fluctuating one, and $-\rho\overline{\grave{u}_i \grave{u}_j}$ are the Reynolds stress which are calculated using eddy viscosity turbulence models as

$$-\rho\overline{u_i' u_j'} = \mu_t\left(\frac{\partial \overline{u_i}}{\partial x_j} + \frac{\partial \overline{U_j}}{\partial x_i}\right) - \frac{2}{3}\rho k\, \delta_{ij} \tag{10}$$

The eddy or turbulent viscosity μ_t was calculated in this study using the shear stress transport SST k-ω model, δ_{ij} is the kronecker second- order tensor given by:

$$\delta_{ij} = \begin{cases} 1 \text{ if } i = j \\ 0 \text{ if } i \neq j \end{cases}$$

The SST k-ω model is an empirical model based on model transport equations for the turbulence kinetic energy *k* and the specific dissipation rateω. Eddy or turbulent viscosity is calculated as:

$$\mu_t = \frac{\rho k/\omega}{max\left(1; \frac{\Omega F_2}{(a_1 \omega)}\right)} \tag{11}$$

In the turbulent boundary layers, the maximum value of the eddy viscosity is limited by forcing the turbulent shear stress to be bounded by the turbulent kinetic energy time a_1. This effect is achieved with the auxiliary function F_2 and the absolute value of vorticity Ω. The auxiliary function F_2 is defined as a function of wall distance y as:

$$F_2 = tanh\left\{\left[max\left(2\,\frac{\sqrt{k}}{0.09\omega y};\frac{500\mu}{\rho y^2\omega}\right)\right]^2\right\} \tag{12}$$

The transport equations as developed by Menter [25] and presented by Bardina et al. [26] are:

$$\frac{\partial}{\partial x_j}\left[\rho k\overline{u_j} - (\mu + \sigma_k\mu_t)\frac{\partial k}{\partial x_j}\right] = \tau_{ij}S_{ij} - \beta^*\rho\omega k \tag{13}$$

$$\frac{\partial}{\partial x_j}\left[\rho\omega\overline{u_j} - (\mu + \sigma_\omega\mu_t)\frac{\partial \omega}{\partial x_j}\right] = P_\omega - \beta\rho\omega^2 + 2(1-F_1)\frac{\rho\sigma_{\omega 2}}{\omega}\frac{\partial k}{\partial x_j}\frac{\partial \omega}{\partial x_j} \tag{14}$$

P_ω is the production term of ω and the function F_1 is designed to blend the model coefficient in the boundary layer zones. The constants of the model are a_1 and β^*. Model coefficients are β, γ', σ_k and σ_w. Complete details on the model can be obtained from the original papers

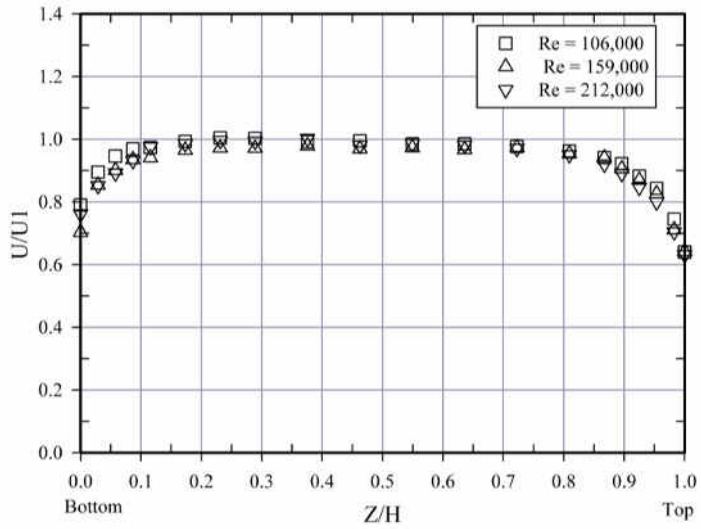

Fig. 5. Inlet velocity profile

3.2. Boundary conditions

The velocity profile of the incoming flow was obtained from the current experimental measurements and was applied at the inlet boundary for different Reynolds numbers

considered in this study. Figure 5 shows the inlet velocity profiles at inlet velocities of 10, 15, and 20 m/s corresponding to inlet Reynolds numbers of 106000, 159000 and 212000, respectively. The figure shows that the inlet velocity profile is essentially uniform between 0.2 and 0.75blade height. The turbulence intensity was set at inlet as 1% as measured in the present study while the turbulence length scale was considered as 0.001 mm based on the general guidelines for CFD calculation [27]. The inlet temperature was considered as the measured ambient temperature at T_∞ = 290K. The non-slip wall boundary condition was considered at the blade surface and at the end-wall. Constant heat flux boundary condition was considered at the blade surface obtained from the experimental procedure.

3.3. Grid generation

The three-dimensional unstructured grid was generated using the preprocessor software Gambit, release 2.3.16. A two-dimensional mesh was generated to solve the mid-span flow and to obtain the appropriate near wall distance corresponding to dimensionless wall distance y^+ smaller than 1 which is necessary to solve the viscous sub-layer. The two-dimensional grid was created using unstructured topology with quadrilateral elements. A boundary layer region was used around the blade consisting of structured O- type mesh to allow fine grid near the solid walls. Several trials were performed until the dimensionless wall distance y^+ was achieved smaller than 1 which is a prerequisite for the solution of the viscous sub-layer and heat transfer near the walls. The volume mesh was created by copying the two-dimensional grid in the span-wise direction. Boundary layer zones were also specified at the end-wall to solve the flow near the wall. Figure 6 shows the computational grid.

3.4. Grid independence study

The solution grid dependency was examined at inlet Reynolds number of 106000. Four grids were used to check the grid dependency with total numbers of cell of 661160, 1090914, 1652900, and 1818190 for the half span. The effect of grid size on the local heat transfer coefficient was examined. The calculations indicated that for all grid sizes, the mid-span heat transfer showed grid independent solution.

The comparison at the level corresponding to span-wise distance of 0.125H showed also grid independent results. However, the span-wise distance corresponding to 0.25 H showed grid dependence on the blade suction surface. Figure 7 shows the comparison between Nusselt number obtained using different grid sizes. The figure indicates that there is no significant change in Nusselt number when the mesh size increased above 1652900. Except the S/c = 0.8638, and 0.9538 points on suction side, as increasing the total number of cell from 1652900 to 1818190 the Nusselt number increases by 0.48% and 1.89% for S/c =

0.8638, and S/c = 0.9538 respectively. Therefore, grid independent solution was obtained with almost 1652900 cells for the blade half span.

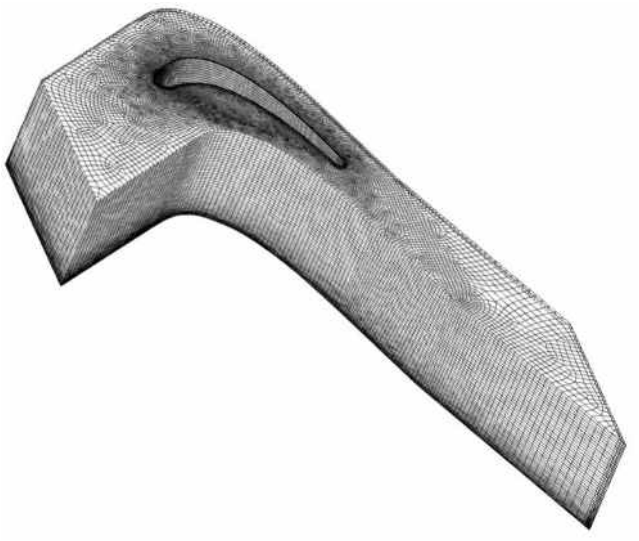

Fig. 6. Computational grid

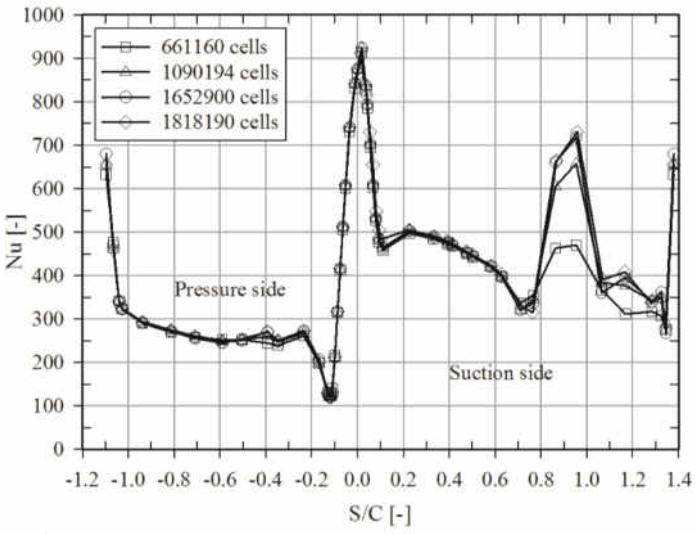

Fig. 7. Heat transfer coefficients for different meshes

4. Results and discussion

4.1. Blade three-dimensional heat transfer

Figure 8 shows Nusselt number distribution along blade surface at different locations through blade height for inlet Reynolds number of 106000. The local Nusselt number is presented as a function of the dimensionless distance along blade surface (S/C). The figure indicates that the maximum Nusselt number was predicted at the stagnation point. Then, Nusselt number decreases on both blade sides. Generally, Nusselt number is higher on the blade suction surface than on the blade pressure surface. This is caused by the high velocity on the blade suction surface corresponding to the low pressure compared to the relatively low velocity and the associated Nusselt number on the blade pressure surface.

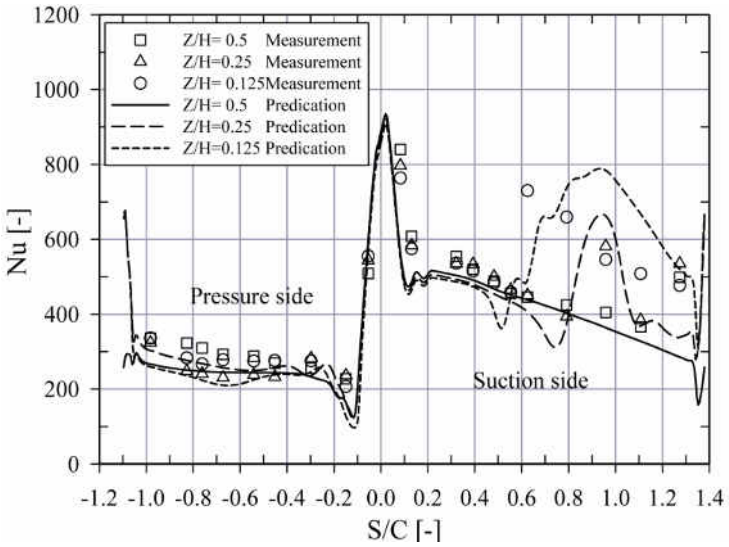

Fig. 8. Nusselt number distribution on the blade surface at different span-wise locations, Re=106000

On the pressure surface, Nusselt number sharply decrease near S/C = -0.1. The reduction in Nusselt number close to blade leading edge it extensively discussed by Choi et al [8] which was attributed to laminar flow separation, and flow reattachment on that region of pressure surface. After flow reattachment and accelerates, it gradually increases from S/C = -0.1 to trailing edge. At blade mid-span on the suction surface, Nusselt number decreased after the stagnation point due to boundary layer growth. The increase in Nusselt number past S/C = 1.1 may be attributed to laminar to turbulent transition. In the region near the endwall of suction side namely at Z/H = 0.25, and 0.125, the secondary flow has a dominate effect on Nusselt number. The decelerating flow region (adverse pressure

gradient) evident in figure 9, near S/C ≅ 0.4, from this point on, the effects of secondary flow are evident. Heat transfer is affected by the vortex structures described by Langston et al. [12], Sieverding [13] and Wang et al. [14]. The passage vortex and the pressure side leg of the horseshoe vortex approach the suction side region. Nusselt number is enhanced by secondary flow impinging on the end-wall region of suction surface as shown in figure 10. The vortices lift off the end-wall and approach the 25% span. Previous measurements showed that the vortices exit the turbine blade at 50% mid-span Giel et al. [15].

This result is obtained by experimental measurements and confirmed by the numerical calculations. Examining wall static pressure on the blade surface Figure 9, indicates that

the flow is accelerating on the blade pressure surface from the $^{S}/_{C} = 0.0$ to the trailing edge. The increase in the local velocity increases the local Nusselt number on the blade pressure surface. However, the development of the boundary layer induces thermal resistance. These two counter effects resulting almost constant Nusselt number on the pressure surface. On the blade suction surface, the flow is accelerating to the location of S/C=0.4, then the flow is decelerating.

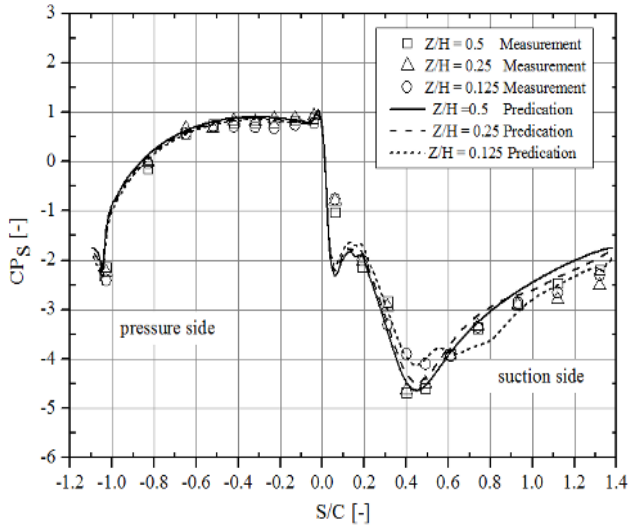

Fig. 9. Blade static pressure coefficient at different span-wise locations and at Re = 106,000

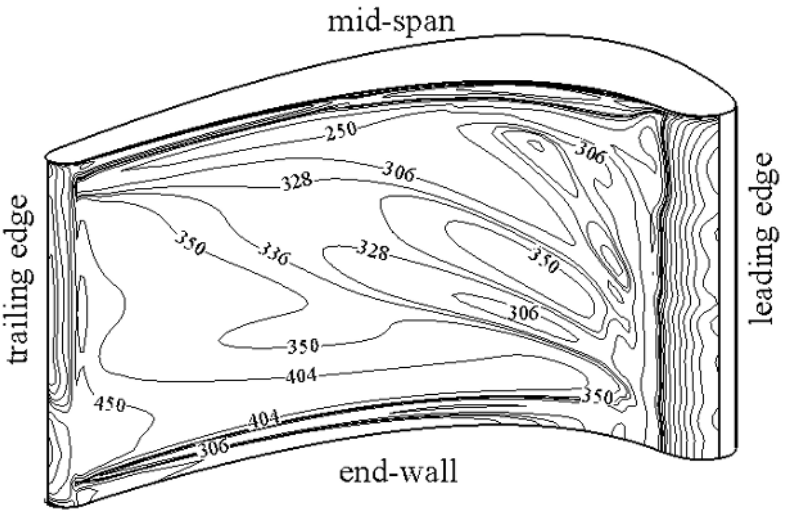

a) Pressure side

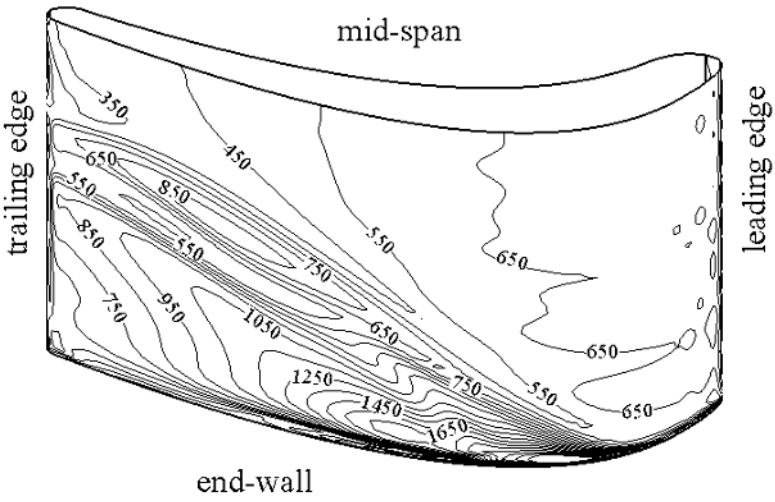

b) Suction side

Fig. 10. Surface limiting streamlines superimposed on Nusselt number, Re=106000

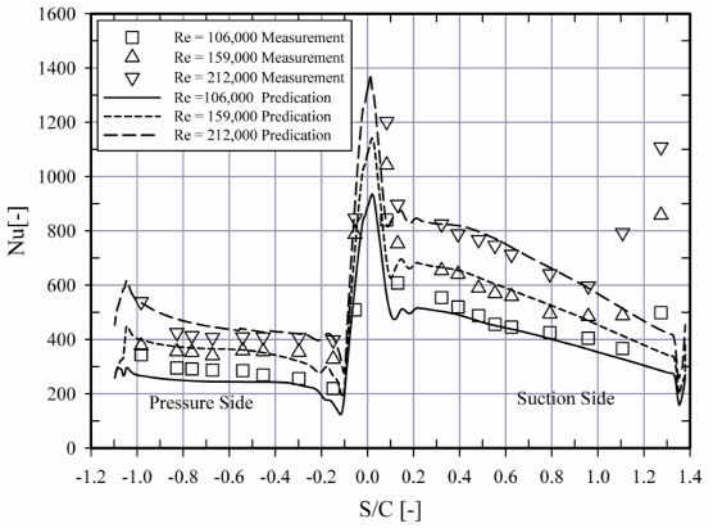

Fig. 11. Effect of Reynolds number on mid-span heat transfer

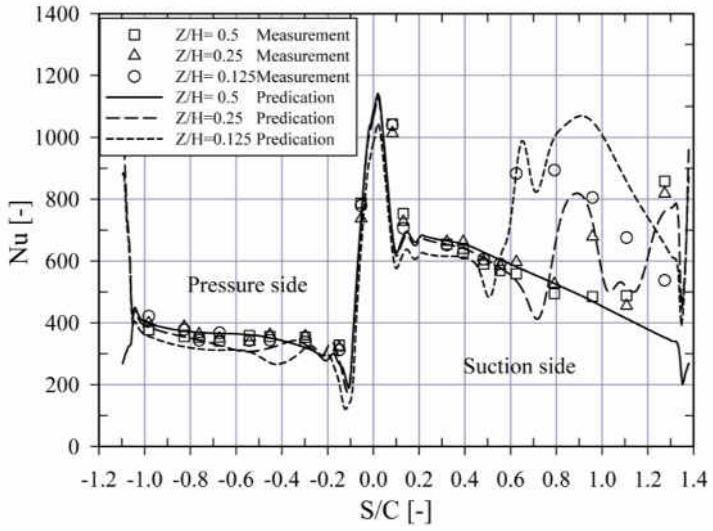

Fig. 12. Nusselt number distribution at different locations through blade height, Re =159000

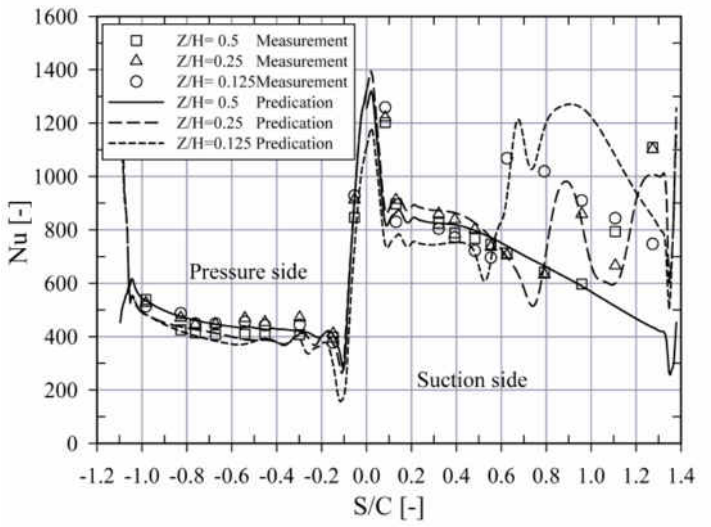

Figure 13. Nusselt number distribution at different locations through blade height, Re = 212,000

Figure 10 shows contour plots of Nusselt number on blade pressure and suction surfaces. High Nusselt number was predicated at the blade leading edge and decreased sharply downstream on the pressure side due to boundary layer growth. Nusselt number results on the blade suction surface had the feature of a triangle region with enhanced Nusselt number located after blade mid-chord near the blade end-wall surface. The enhanced Nusselt number is due to the action of the passage vortex, as explained above. A close examination of the triangular region shows two separate regions of high Nusselt number, separated by a lower Nusselt number line. A large region of the enhanced heat transfer is caused by the action of passage vortex that has been drawn toward the suction surface. Above this region, a high heat transfer is caused by the action of the suction side vortex. This agrees well with the flow visualizations of Wang et al. [14].

4.3. Effect of Reynolds number

Figure 11 shows the predicted Nusselt number from the numerical calculations and the experimentally measured local Nusselt number on blade mid-span at different inlet Reynolds number namely 106000, 159000, and 212000. The figure shows that good agreement was obtained between numerical predictions and experimental measurements. Generally, increasing Reynolds number increases Nusselt number distribution at different locations from the blade leading edge to trailing edge. The experimental measurements show that Nusselt number increased sharply at about S/C=1.1 which could not be predicted by the numerical calculations. The possible reason for this discrepancy is the absence of

the transition modeling in the numerical calculation. The increase in heat transfer at this location at high Reynolds number could also be attributed to flow separation.

Figures 12 to 13 show the measurement and predicated Nusselt number distribution at different levels through blade height and at Reynolds numbers of 159000, and 212000 respectively. The figures show good agreement between numerical model predictions and the experimental measurements. The same trend of Nusselt number is obtained at different Reynolds numbers. However, increasing Reynolds number increases blade heat transfer. The increase in the local Nusselt number on the blade suction near the trailing edge at

$Z/H = 0.25$ and 0.125 is also obtained from the measurements and confirmed by the numerical calculations. These figures indicates also that Reynolds number affects the magnitude of heat transfer on the blade pressure and suction surfaces but the distribution of heat transfer coefficient does not depended on Reynolds number

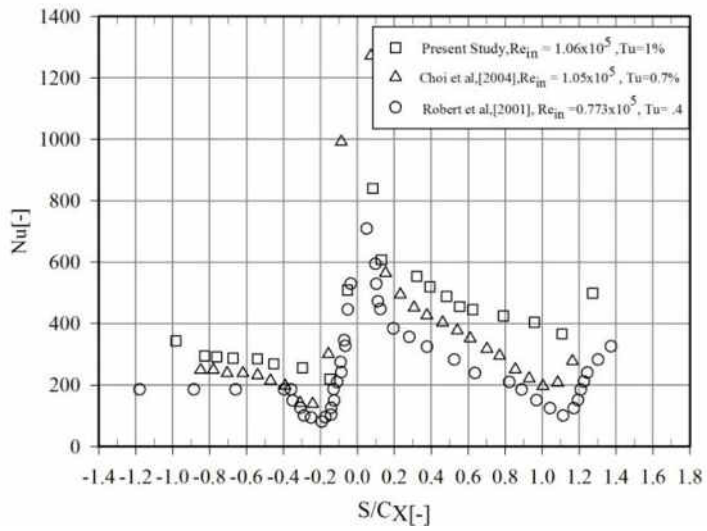

Fig. 14. Comparison of local Nu distributions at mid span region.

Figure 14 shows the comparison of the Nusselt number at midspan region in the present study and in other researcher's experiments. For the exact comparison, the data for relatively low Reynolds numbers (the order of 10^5) are taken for all cases. For the comparison with the present results, the levels and the Nusselt number are fairly similar, although some discrepancies are observed in certain regions because of the different blade profile and flow conditions.

5. Conclusions

Three-dimensional heat transfer measurements and numerical calculations were performed in this study to investigate the effect of the secondary flow on the heat transfer

through turbine blades. The numerical calculations showed reasonable agreements with the experimental measurements. It was found through the study that the secondary flow increases heat transfer on the blade suction surface near the blade trailing edge. Separation line was predicted by the numerical technique on the blade suction surface corresponding to the passage vortex. The separation line is characterized by high heat transfer rates. Increasing Reynolds number changes the magnitude of heat transfer coefficients keeping the same heat transfer pattern unchanged.

6. Nomenclature

a_1 = constant

C = chord length

C_x = axial chord

C_p = static pressure coefficient,

F_1, F_2= functions

h = local heat transfer coefficient

H = blade height

k = turbulent kinetic energy

K = air thermal conductivity

Nu = Nusselt number

P_s = static pressure

P_ω = production of ω

P = blade pitch

q'' = local convective heat flux

q''_{gen} = generated heat flux

q''_{loss}= loss heat flux

q''_c = loss heat flux by conduction

Re = Reynolds number

S = Distance along blade surface

S_{ij} = mean strain rate tensor

T_w = steady state strip temperature

T_∞ = temperature at cascade inlet

u' = fluctuating velocity

$\bar{u}$ = mean velocity

U = mass-averaged velocity

x_j = coordinate in j-th direction

x = distance through axial chord

x_1, x_2= independent variables

y = distance along blade spacing

y^+ = dimensionless wall distance

Z = distance along blade height

Greek Symbols

β_1 = inlet blade angle

β_2 = exit blade angle

β, γ'= model coefficients

β^* = model constant

ϵ = emissivity

μ = molecular viscosity

μ_t = turbulent eddy viscosity

ω = specific turbulent dissipation rate

Ω = magnitude of mean vorticity

ρ = fluid density

σ = Stefan Boltzmann constant

σ_k, σ_ω= model coefficients

τ_{ij} = turbulent Reynolds stresses

Subscripts

1 = inlet
2 = exit

i, j = tensor indices

7. References

[1] Arts, T., DeRouvroit, M.L., and Rutherford, A.W., Aero- thermal investigation of a highly loaded transonic linear turbine guide vane cascade, VKI- Technical Note-174,1990.
[2] Harasgama, S. P., Tarada, F. H., and Baumann, R., Calculation of heat transfer to turbine blading using two- dimensional boundary layer methods, ASME, 1993, paper GT1993-79.
[3] Jiasen, H.U., and Fransson, T.H., On the application of transition correlations in turbomachinery flow calculation, ASME, 1998, paper GT1998- 460.
[4] Pecnik, R. and Sanz, W., Application of the turbulent potential model to heat transfer predictions on a turbine guide vane, ASME Journal of Turbomachinery, 2007, Vol. 129, pp. 628- 635.
[5] Liu, Y., Aerodynamics and heat transfer predictions in a highly loaded turbine blade, International Journal of Heat and Fluid Flow, 2007, vol. 28, pp. 932- 937.
[6] Zhang, L., and Han, J.C., Influence of mainstream turbulence on heat transfer coefficients from a gas turbine blade, ASMEJ. Heat Transfer,1994, Vol. 116, pp. 896–903.
[7] Robert, J. B., Aaron R. B., Kenneth, V. T., and James, W. B., The effect of turbulence intensity and length scale on low-pressure turbine blade aerodynamics, International Journal of Heat and Fluid Flow, 2001, vol. 22, pp.123- 133.
[8] Choi, J., Teng,C., Han, J.C., and Ladeinde, F., Effect of free-stream turbulence on turbine blade heat transfer and pressure coefficients in low Reynolds number Flows, International Journal of Heat and Mass Transfer, 2004, Vol. 47, pp. 3441–3452.
[9] Nix, A. C., Diller,T. E., Ng, W. F., Experimental measurements and modeling of the effects of large-scale freestream turbulence on heat Transfer, ASME Journal of Turbomachinery,2007, Vol. 129, pp. 542- 550.

[10] Nasir, S., Carullo, j. S., Wing, F. N.,Thole, K. A., Hong,W., Effects of large scale high free stream turbulence and exit Reynolds number on turbine Vane heat transfer in a transonic cascade, ASME Journal of Turbomachinery, 2009, Vol. 131, pp. 1- 11.

[11] Garg, V. K., and Ameri, A. A., Two-equation turbulence models for predication of heat on a transonic turbine blade, International Journal of Heat and Fluid Flow, 2001, Vol. 22, pp. 593-602.

[12] Langston, L.S., Nice, M.L., and Hooper, R.M., Three-dimensional flow within a turbine cascade passage, Journal of Engineering Power, Transaction of ASME, January 1977, pp.21-28.

[13] Sieverding, C.H, Recent progress in the understanding of basic aspects of secondary flows in turbine blade passages, Journal of Engineering for Gas Turbines and Power, Transactions of ASME, Vol. 107, April 1985, pp. 248-257.

[14] Wang, H. P., Olson, S. J., Goldstein, R. J., and Eckert, E. R. G., Flow visualization in a linear cascade of high performance turbine blades ASME Journal of Turbomachinery, 1997, Vol. 119, pp. 1-8.

[15] Giel, P.W., Van Fossen, G.J., and Boyle, R.J., Blade heat transfer measurements and predications in a transonic turbine cascade, NASA/ TM- 1999-209296.

[16] Pecnik, R., Pieringer, P., and Sanz, S., Numerical investigation of the secondary flow of a transonic turbine stage using turbulence closures, ASME, 2005, paper GT2005- 68754.

[17] Johan, H., Valery, C., Jonas, L., Lennart,L., Numerical validations of secondary flows and loss development downstream of a highly loaded low pressure turbine outlet guide vane cascade, ASME, 2007, paper GT2007-27712.

[18] Papa, M., Influence of Blade Leading Edge Geometry and Upstream Blowing on the Heat/Mass Transfer in a Turbine Cascade, Ph.D., University of Minnesota, April 2006.

[19] Lee, S. W., Park, J. J., Effects of incidence angle on endwall convective transport within a high turning rotor passage, International Journal of Heat and Mass Transfer, 2009, vol. 52,pp.5922-5931.

[20] Lynch, S. P., Sundaram, N., Thole, K. A., Kohli, A., Lehane, C., Heat transfer for a turbine blade with nonaxisymmetric endwall contouring, ASME Journal of Turbomachinery, 2011, vol. 133, pp. 0110019-1-011019-9.

[21] Lynch, S. P., Thole, K. A., Kohli, A., Lehane, C., Computational predictions of heat transfer and film cooling for a turbine blade with nonaxisymmetric endwall contouring, ASME Journal of Turbomachinery, 2011, vol. 133, pp. 041003-1-041003-10.

[22] Morata, E. C., Gourdain, N., Duchaine, F., and Gicqel, L.Y.M., 2012, Effects of free stream turbulence on high pressure turbine blade heat transfer predicated by structured and unstructured LES, International Journal of Heat and Mass Transfer,55 (2012) 5754-5768

[23] El-Batsh, H., Effect of the radial pressure gradient on the secondary flow generated in an annular turbine cascade, International Journal of Rotating Machinery, 2012, Article ID 509209, 14 pages.

[24] Holman, J.P., Gajda, W.J. Experimental method for engineering, McGraw Hill, New York, 1989.

[25] Menter, F., Two-equation eddy-viscosity turbulence models for engineering applications, AIAA Journal, vol. 32 (8), pp. 1598-1605, 1994.

[26] Bardina, J.E.; Huang, P.G. and Coakley, T.J., Turbulence modeling validation, testing and development, NASA technical memorandum 110446, 1997.

[27] Casey, M. and Wintergerste, T., ERCOFTAC special interest group on quality and trust in industrial CFD, Best Practices Guidelines, 2000.

خصائص انتقال الحرارة الثلاثى الأبعاد خلال مصفوفة خطية لريش التربينات

الملخص:

تتناول هذه الدراسة على فحص معملى وعددى لخصائص إنتقال الحرارة الثلاثى الابعاد خلال ريشة تربينة. تم خلال هذه الدراسة بناء جهاز معملى مكون من مصفوفة خطية مكونة من خمس مسارات لريش التربينات. كما تم قياس معدلات انتقال الحرارة للقناه المتوسطة عند التأثير على الريش بكمية حرارة متماثلة حيث تم تسخين الريشة بإستخدام تسعة وعشرون شريحة تسخين كهربية مثبتة رأسيا على السطح الخارجى للريشة. تم قياس معدلات انتقال الحرارة على ثلاث مستويات على ارتفاع الريشة باستخدام ازدواج حرارى. علاوة على ذلك فقد تم قياس توزيع الضغط الاستاتيكى على سطح الريشة لفهم خصائص انتقال الحرارة. كما تم استخدام حسابات عددية لفهم السريان وانتقال الحرارة عند المواضع التى لم يتم القياس فيها. تم حل معادلات الحركة للسريان الثلاثى الابعاد والمضطرب والمكونة من معادلة الاستمرارية ومعادلات كمية الحركة ومعادلة الطاقة بالاضافة لمعادلات الدوامات. تم التوصل من خلال هذه الدراسة الى ان السريان الثانوى يعمل على زيادة معدلات انتقال الحرارة على سطح السحب للريشة. كما تم التنبؤ بمعدلات انتقال حرارة مرتفعة عند خطوط انفصال السريان من الحسابات العددية والتى توافقت بصورة جيدة مع القياسات المعملية.